

Measurement report: Brown carbon aerosol in rural Germany: sources, chemistry, and diurnal variations

Feng Jiang^{1,2,a}, Harald Saathoff^{1*}, Uzoamaka Ezenobi¹, Junwei Song¹, Hengheng Zhang¹, Linyu Gao¹, and Thomas Leisner^{1,3}*

¹Institute of Meteorology and Climate Research, Karlsruhe Institute of Technology, 76344 Eggenstein–Leopoldshafen, Germany

²Institute of Applied Geosciences, Working Group for Environmental Mineralogy and Environmental System Analysis, Karlsruhe Institute of Technology, 76131 Karlsruhe, Germany

³Institute of Environmental Physics, Heidelberg University, 69120 Heidelberg, Germany

^anow at: Paul H. O'Neill School of Public & Environmental Affairs, Indiana University, Bloomington, Indiana 47405, United States

Correspondence to: Feng Jiang (feng.jiang@kit.edu) and Harald Saathoff (harald.saathoff@kit.edu)

Abstract. Brown carbon aerosol (BrC) is one major contributor to atmospheric air pollution in Europe, especially in winter. Therefore, we studied the chemical composition, diurnal variation, and sources of BrC from 17th February to 16th March 2021 at a rural location in southwest Germany. In total, 178 potential BrC molecules (including 7 nitro aromatic compounds, NACs) were identified in the particle phase comprising on average $83 \pm 44 \text{ ng m}^{-3}$, and 31 potential BrC (including 4 NACs) molecules were identified in the gas phase contributing on average $8.5 \pm 6.7 \text{ ng m}^{-3}$ during the whole campaign. The average light absorption of seven NACs in the particle phase was $0.2 \pm 0.2 \text{ Mm}^{-1}$, contributing to $2.2 \pm 2.1\%$ of total BrC absorption at 370 nm. The 178 potential BrC molecules only accounted for $2.6 \pm 1.5\%$ of the total organic mass, but can explain $14 \pm 13\%$ of the total BrC absorption at 370 nm, assuming an average mass absorption coefficient at 370 nm (MAC_{370}) of $9.5 \text{ m}^2 \text{ g}^{-1}$. A few BrC molecules dominated the total BrC absorption. In addition, diurnal variations show that gas phase BrC was higher at daytime and lower at night. It was mainly controlled by secondary formation (e.g., photooxidation) and particle-to-gas partitioning. Correspondingly, the particle phase BrC was lower at daytime and higher at nighttime. Secondary formation dominates the particle-phase BrC with $61 \pm 21\%$, while $39 \pm 21\%$ originated from biomass burning. Furthermore, the particle-phase BrC showed decreasing light absorption due to photochemical aging. This study extends the current understanding of real-time behaviors of brown carbon aerosol in the gas and particle phase at a location characteristic for the central Europe.

29 **1. Introduction**

30 The Brown Carbon (BrC) aerosol has significant impact on air quality and climate, since it absorbs the solar radiation
31 in the near-ultraviolet and visible region (Laskin et al., 2015; Moise et al., 2015). Global simulation showed that the
32 mean radiative forcing of BrC aerosol was -0.43 W m^{-2} and 0.05 W m^{-2} at the surface and at the top of the atmosphere,
33 accounting for 15% of total radiative forcing by the absorbing aerosol (Park et al., 2010). In addition, global
34 measurements of BrC found that the average direct radiative effect of BrC absorption accounted between 7% to 48%
35 at the top of the atmosphere (Zeng et al., 2020).

36 Some typical molecules of BrC have been identified, such as nitro-aromatic compounds (NACs), imidazoles, and
37 polycyclic aromatic hydrocarbons (PAH), etc., (Jiang et al., 2022; Wu et al., 2018; Huang et al., 2018; Liu et al., 2023).

38 In western Europe, the concentration levels of NACs range between $1\text{--}20 \text{ ng m}^{-3}$, accounting for 0.3%–4% of total
39 absorption of BrC at UV wavelengths (Jiang et al., 2022; Mohr et al., 2013; Teich et al., 2017). In addition, imidazoles
40 were detected with concentrations ranging between $0.2\text{--}14 \text{ ng m}^{-3}$ in ambient aerosol samples from different
41 environments in Europe and China (Teich et al., 2016). Furthermore, parent-PAHs and carbonyl-OPAHs accounted
42 for on average $\sim 1.7\%$ of the overall absorption of methanol-soluble BrC in Urban Xi'an, Northwest China (Huang et
43 al., 2018). Even though many studies have investigated the chemical composition of brown carbon and calculated the
44 absorption contribution from BrC molecules, there are still many unknown brown carbon molecules to allow a
45 quantitative assessment of their sources and atmospheric impact.

46 Sources of BrC can be separated as primary emissions and secondary formation. The primary sources of BrC are
47 biomass burning and fossil fuel combustion (Andreae and Gelencser, 2006). On a global scale, a majority of BrC
48 aerosol mass is associated with biomass burning dominating BrC absorption (Zeng et al., 2020). The major secondary
49 sources of brown carbon are from oxidation of aromatic volatile organic compounds, such as toluene (Lin et al., 2015),
50 naphthalene (Siemens et al., 2022), ethylbenzene (Yang et al., 2022), and indole (Montoya-Aguilera et al., 2017; Jiang
51 et al., 2024), especially in the presence of NO_2 .

52 BrC in the atmosphere can be suspended in the gas phase or particle phase. However, only a few studies have
53 investigated the sources and chemical composition of BrC in the gas phase. For example, NACs in the gas phase were
54 highest during the daytime at a rural site in China (Salvador et al., 2021). The major sources of NACs were from
55 secondary formation on days without extensive biomass burning emissions, but mainly from primary emissions in
56 biomass burning events (Salvador et al., 2021). The source of nitrophenol, a typical BrC molecule, was mainly from
57 secondary formation outweighing losses by photolysis in polluted urban environments, Beijing (Cheng et al., 2021).

58 The major chromophores of BrC in the gas phase were rich in phenol- and protein-like substances in Xi'an, China,
59 during the summer (Chen et al., 2021). Therefore, the previous studies mainly focus on sources and chromophores of
60 BrC, especially NACs. However, the real-time diurnal variation and sources of BrC in the gas phase in the atmosphere
61 have rarely been investigated in central Europe.

62 Previous field studies have investigated the sources of BrC in the particle phase which are mainly from secondary
63 formation and primary emissions (Wang et al., 2019a; Moschos et al., 2018; Satish et al., 2017). In the central Europe,
64 the secondary biogenic organic aerosol (OA) contributes less BrC in summer. However, the primary and secondary
65 wood burning emissions dominated the BrC (Moschos et al., 2018). The primary emissions of BrC contributed more
66 to organic aerosol light absorption than those from secondary processes in the North China Plain, China (Wang et al.,
67 2019a). However, secondary sources for BrC were more important for absorption than primary ones in the Southeastern
68 Margin of Tibetan Plateau (Wang et al., 2019b). Loss pathways of BrC in the particle phase mainly comprise
69 photooxidation and photobleaching, but also dilution of BrC e.g. by rising boundary layer height influences its
70 concentration levels (Satish et al., 2017; Laskin et al., 2015; Moise et al., 2015). The absorption of BrC was high in
71 the early morning and later decreased due to the bleaching of chromophores (Wang et al., 2019a; Satish et al., 2017).
72 A diurnal cycle showed that secondary chromophores can be formed from photochemical oxidation after sunrise
73 followed by photobleaching of the chromophores under the oxidizing conditions as the day progressed (Wang et al.,
74 2019b). Lower BrC concentrations during noon were explained by the fact that planetary boundary layer heights were
75 highest during the middle of the day (Liu et al., 2023). However, also nighttime aqueous-phase chemistry can promote
76 the formation of secondary light absorbing compounds and the production of strongly absorbing particles (Wang et al.,
77 2019a). In addition, higher emissions of biomass burning BrC were observed at nighttime. Actually, the BrC in the
78 particle phase undergoes complex photochemical processing during the whole day. The time dependent sources and
79 diurnal variations of BrC in aerosol particles are still reported rarely and not well understood.

80 To better understand the chemical characterization, diurnal variation, and sources of BrC in central Europe, we
81 performed online measurements of BrC during February-March 2021 at a rural location in southwest Germany. In the
82 following, we will describe the experimental methods used in this study. Subsequently, the mass concentrations of BrC
83 in gas and particle phase will be determined. Furthermore, the contribution of BrC to light absorption in the particle
84 phase will be estimated. Then, the diurnal variations and sources of BrC in the gas and particle phase will be analyzed.
85 Finally, the atmospheric implications of our findings will be discussed.

86 **2. Experimental methods**

87 **2.1. Measurement site**

88 We performed particle and trace gas measurements from February 17th–March 16th 2021 at KIT Campus Nord, a rather
89 rural area in Germany (49°05'43.1"N 8°25'45.6"E). The sampling site is located at the building number 322 of the
90 IMK-AAF on KIT Campus Nord, as shown in Figure S1. The campus is mostly surrounded by the Hardwald forest
91 dominated by pine trees. The sampling site is also near some villages e.g. 3–4 km east of the village “Eggenstein-
92 Leopoldshafen”, 6–7 km northeast of the village “Neureut”, 3–4 km west of the village “Friedrichstal”, 4–5 km
93 northwest of the village “Stutensee”, and 5–6 km southeast of the village “Linkenheim”. Therefore, influences by
94 biomass burning emissions from wood stove combustion in these residential areas during winter time can be expected
95 (Thieringer et al., 2022). Furthermore, the city of Karlsruhe with 3000000 inhabitants is 10 km south of the
96 measurement site. The city includes industrial areas with a coal-fired power plant “Rheinhafen” and a refinery “MIRO”.
97 Therefore, the measurement site is potentially affected by different aerosol sources.

98 **2.2. Meteorological, aerosol particle, and traces gas instruments**

99 All instruments were set up in a temperature-controlled measurement building. The samples were collected above the
100 roof top about 8 m above ground level via stainless steel tubes and a PM_{2.5} and a TSP inlet as well as FEP tubes for the
101 VOC measurements. An overview of the instruments used and the parameters measured is given in Table S1 of the
102 Supplement.

103 Temperature, relative humidity (RH), pressure, wind speed, wind direction, precipitation, and global radiation were
104 measured by a meteorological sensor (WS700, Lufft GmbH; see Table S1) about 8 m above the ground level. The main
105 wind directions during the campaign were southwest, northeast, and southeast, since winds were channeled by the
106 Rhine River valley. O₃ and NO₂ were measured with standard gas monitors (Table S1). The particle number
107 concentrations (>2.5 nm) were measured by a water-based condensation particle counter (CPC3789, TSI Inc.). PM_{2.5}
108 was measured by an optical particle counter (OPC-FIDAS 200, Palas Inc.). The particle number size distributions were
109 measured by a nanoparticle sizer (NanoScan, TSI Inc.) ranging from 10-410 nm at a time resolution of 1 min. Black
110 carbon (BC) concentrations were measured with aethalometers (AE33, Aerosol Magee Scientific).

111 2.3. Online FIGAERO-CIMS measurement and identifications of potential BrC molecules

112 The individual organic compounds in both the gas and particle phase were measured with a filter inlet for gases and
113 aerosols coupled to a high-resolution time-of-flight chemical ionization mass spectrometer (FIGAERO-HR-ToF-CIMS,
114 Aerodyne Research Inc. hereafter CIMS) employing iodide (I⁻) for chemical ionization (Lopez-Hilfiker et al., 2014;
115 Jiang et al., 2022). During the gas-phase measurement, the ambient air was sampled via a fluorinated ethylene
116 propylene (FEP) tube of 4.5 m length (flow rate 8 L min⁻¹, residence time 0.9 s). At the same time, the particles were
117 collected on a Teflon (Polytetrafluoroethylene, PTFE) filter via ~~as~~ separate sampling port connected to a PM_{2.5} inlet
118 (total flow rate 16.7 L min⁻¹) and an 8 m long stainless-steel tube. The loading time and sampling flow of Teflon filters
119 were 30 minutes and 4 L min⁻¹, respectively. At regular intervals (46 min), the gas-phase measurement was switched
120 off and particles on the filter were desorbed by a flow of ultra-high-purity nitrogen (99.9999-%) heated from room
121 temperature to 200 °C over the course of 35 min (Lopez-Hilfiker et al., 2014; Huang et al., 2019~~a~~). The resulting mass
122 spectral signal evolutions as a function of desorption temperature are termed thermograms (Lopez-Hilfiker et al., 2014).
123 Integration of thermograms of individual compounds yielded their signal in counts per second, which were converted
124 to mass concentrations using an average sensitivity of 22 count s⁻¹ ppt⁻¹ (cps ppt⁻¹, ppt: parts per trillion) (Lopez-Hilfiker
125 et al., 2014). First calibrations for nitro aromatic compounds (NACs) were done directly after field campaign. However,
126 due to technical problems, the calibration of 4-nitrophenol, 4-nitrocatechol, 2-methyl-4-nitropehnol, and 4-methyl-5-
127 nitrocatechol was repeated in August 2024~~After the field campaign, the calibration of 4 nitrophenol, 4 nitrocatechol,~~
128 ~~2-methyl-4-nitropehnol, and 4-methyl-5-nitrocatechol was utilized to characterize the sensitivity factor of nitro~~
129 ~~aromatic compounds (NACs), as shown in the Supplement. Despite the large time between measurements and second~~
130 ~~calibration, we have indications from repeated measurements of formic acid that the sensitivity of the instrument didn't~~
131 ~~change substantially over this time period. Please note that this leads to an additional uncertainty of about 20%. The~~
132 ~~sensitivity factors~~ of our iodide CIMS for 4-nitrophenol, 4-nitrocatechol, 2-methyl-4-nitropehnol, and 4-methyl-5-
133 nitrocatechol were 18 ± 10 cps ppt⁻¹, 11 ± 7 cps ppt⁻¹, 21 ± 11 cps ppt⁻¹, and 21 ± 14 cps ppt⁻¹, respectively ~~0.80 ± 0.44,~~
134 ~~0.50 ± 0.32, 0.96 ± 0.52, 0.97 ± 0.63, respectively~~ (Figure S9). The average sensitivity ~~factor~~ of 4 NACs was 18 ± 12
135 cps ppt⁻¹ ~~0.81 ± 0.53~~. We used this average sensitivity ~~factor~~ to calibrate other potential brown carbon molecules in this
136 study. The sensitivity ~~factor~~ of levoglucosan was 9 ± 3 cps ppt⁻¹ ~~0.40 ± 0.14~~ in this study (Figure S10). We used the
137 sensitivity ~~factor~~ of 9 ± 3 cps ppt⁻¹ ~~0.40 ± 0.14~~ to estimate the concentrations of molecules, which are not identified as
138 potential BrC molecules. ~~Please note that the sensitivity of CIMS for different organic compounds varies by a few~~

139 ~~orders of magnitude. Sensitivity uncertainties were taken into account in the calculation of the overall uncertainties of~~
140 ~~CIMS concentrations ($\pm 60\%$) following the approach by Thompson et al. (2017).~~

141 During the measurements, the mass resolution of FIGAERO-CIMS was relatively stable with about 4000 m/ Δ . The
142 interference from isomers with different vapor pressures or thermal fragmentation of larger oligomeric molecules can
143 lead to more complex, multimodal and broader thermograms (Lopez-Hilfiker et al., 2014). The signal integration can
144 include the different isomers or thermal fragmentation of larger oligomers. Therefore, the isomers or thermal
145 decomposition can lead to increase errors of estimating the organic mass concentrations. In this study, BrC molecules
146 were identified and partially quantified in atmospheric aerosol by FIGAERO-CIMS. Please note that the iodide CIMS
147 has sensitivities varying over several orders magnitude for different compounds e.g., of different oxidation states
148 (Lopez-Hilfiker et al., 2016). Therefore, the quantitative interpretation is limited to the small amount of compounds
149 for which we could do calibration with authentic standards. Keeping this in mind, it can still be meaning to a relative
150 comparison of the large number of high oxidized compounds assuming the same sensitivity. The raw data were
151 analysed by using the toolkit Tofware (v3.1.2, Tofwerk, Thun, Switzerland, and Aerodyne, Billerica) with the Igor Pro
152 software (v7.08, Wavemetrics, Portland, OR). Gas phase background was determined by sampling zero air (high purity
153 synthetic air). Particle phase backgrounds were assessed by putting an additional Teflon filter upstream of the particle
154 phase sampling port during the deposition (Huang et al., 2019a; Lee et al., 2018).

155 We observed typically about 1500 mass peaks from particles and 120 mass peaks in gases corresponding to different
156 oxygenated organic compounds by using FIGAERO-CIMS. Individual compounds were assigned to the mass peaks
157 by fitting, $C_cH_hO_oN_n$, different numbers of atoms: c carbon, h hydrogen, o oxygen, n nitrogen (Lopez-Hilfiker et al.,
158 2014). A double bond equivalent (DBE) can be calculated as follows (Daumit et al., 2013):

$$159 \quad DBE = \frac{n-h}{2} + c + 1 \quad (1)$$

160 Lin et al., (2016, 2018) employed high-resolution mass spectrometry to analyze biomass burning organic aerosol. They
161 assigned potential brown carbon compounds according to the correlation of double bond equivalents (DBE) with the
162 number of carbon atoms per molecule (Figure S12). We used this method to assign 178 potential BrC molecules
163 (including 7 NACs) in the particle phase and 31 potential BrC molecules (including 4 NACs) in the gas phase, as
164 shown in Figure 1 in the corresponding mass spectra. The gas-to-particle phase partitioning coefficients of those semi
165 volatile potential brown carbon molecules which could be measured in both phases with sufficient sensitivity are listed
166 in table S6. A few other studies also used this method ~~also~~ to assign more brown carbon molecules. For example, good

167 correlations ($r = 0.9$) between mass absorption efficiency at 365 nm and potential brown carbon molecules of larger
168 molecular weight were found by Tang et al., (2020). Xu et al., (2020) used this method to assign 149 nitrogen-
169 containing potential BrC chromophores at the Tibetan Plateau and we used this method to assign potential BrC
170 molecules in downtown Karlsruhe (Jiang et al., 2022). The potential BrC molecules we assigned according to this
171 method for the particle and the gas phase are listed in Tables S2 and S3.

172 **2.4. Particle light absorption from aethalometer measurements**

173 In the aethalometer AE33 (Magee Scientific), aerosol particles are continually sampled on a quartz filter and the optical
174 attenuation is measured with time resolutions of 1 minute at seven wavelengths (370, 470, 520, 590, 660, 880, and 950
175 nm) during this campaign. The light absorption at seven wavelengths was calculated from the measured attenuation.
176 Attenuation is measured on two spots with different sample flows and on the reference spot without sample flow. The
177 two loading spots with different flow are used to allow for loading effect corrections (Drinovec et al., 2015). Since our
178 aethalometer has been used with two loading spots, the loading effect was corrected by a Dual-spot loading
179 compensation algorithm (Drinovec et al., 2015). To further address the scattering effect (Yus-Díez et al., 2021), we
180 did comparison experiments in the Aerosol Preparation and Characterization (APC) chamber (Huang et al., 2018).
181 Black carbon was injected into the APC chamber by using the PALAS soot generator (GfG 1000, Palas) (Saathoff et
182 al., 2003). The APC chamber was connected to a photoacoustic spectrometer (PAS) operating at three wavelengths
183 (405, 520, and 658 nm) (Linke et al., 2016) and an aethalometer (AE33). As shown in Figure S11, for three wavelengths
184 (370, 520, and 660 nm), the correlation slopes were 1.88, 1.94, and 1.98, respectively. The average multiple-scattering
185 correction factor was 1.90 ± 0.06 in this study.

186 The BC mass concentration is calculated from the change in optical attenuation at 880 nm in the selected time interval
187 using the mass absorption cross section $7.77 \text{ m}^2 \text{ g}^{-1}$ (Gundel et al., 1984), since other aerosol particles (organic aerosol
188 or mineral) have less absorption at this wavelength and major absorption is contributed from BC alone. The attenuation
189 mass absorption coefficients of AE33 from 370—880 nm were 18.47, 14.54, 13.14, 11.58, 10.35, and $7.77 \text{ m}^2 \text{ g}^{-1}$,
190 respectively. The absorption measurements by an aethalometer have the filter-based lensing effect (Moschos et al.
191 2021). According to previous studies, the uncertainty from the lensing effect for BC and BrC measurement waswere
192 8%-27% and 6%-20%, respectively (Moschos et al., 2021). We assumed an AAE_{BC} value of 1.0 in this study. However,
193 this assumption introduces an uncertainty in the estimations of BC and BrC light absorptions. According to previous
194 studies, the AAE_{BC} ranges between 0.8 and -1.4 (Lack and Langridge 2013). This range, although maybe not fully

195 applicable to our measurement location, potentially causes relatively large uncertainties of up to 81% (at 370 nm) in
 196 splitting between BrC and BC absorption (Figure S13) (Duan et al. 2024). Despite these potentially large uncertainties
 197 on absolute absorption values, we consider this method still useful. Our assumption of $AAE_{BC} = 1.0$ is reasonable for
 198 our location as based on previous measurements, and it should still allow to discuss the relative evolution of BC and
 199 BrC absorption.

200 -We assumed that the absorption from dust and other aerosol was negligible. Hence, the absorption was only
 201 contributed from BC and BrC. Therefore, $Abs(\lambda)$ can be divided in BC and BrC absorption:

$$202 \quad Abs = Abs_{BrC}(\lambda) + Abs_{BC}(\lambda) \quad (2)$$

203 where $Abs_{BrC}(\lambda)$ is the absorption caused by BrC at the following aethalometer wavelengths, $\lambda = 370, 470, 520, 590,$
 204 or 660 nm while $Abs_{BC}(\lambda)$ is the absorption contributed by BC at the same wavelength (Wang et al., 2019a). To
 205 determine $Abs_{BC}(\lambda)$ at each wavelength, we assumed that BC was the only absorber at $\lambda = 880$ nm, and thus the $Abs_{BC}(\lambda)$
 206 ($\lambda = 370, 470, 520, 590,$ and 660) can be extrapolated from the following equation:

$$207 \quad Abs_{BC}(\lambda) = Abs_{880} \times \left(\frac{\lambda}{880}\right)^{-AAE_{BC}} \quad (3)$$

208 where AAE_{BC} represents the spectral dependence of $Abs_{BC}(\lambda)$, and a value of 1.0 was chosen for AAE_{BC} based on
 209 previous studies in Germany (Teich et al., 2017). Finally, one can obtain the $Abs_{BrC}(\lambda)$ as follows:

$$210 \quad Abs_{BrC}(\lambda) = Abs(\lambda) - Abs(880) \times \left(\frac{\lambda}{880}\right)^{-AAE_{BC}} \quad (4)$$

211 The fraction of wood burning black carbon (BC_{wb}) was calculated by using the aethalometer model (Sandradewi et
 212 al., 2008a; Sandradewi et al., 2008b):

$$213 \quad BC_{wb} = \left[\frac{b_{abs}(470nm) - b_{abs}(950nm) \times \left(\frac{470}{950}\right)^{-\alpha_{ff}}}{\left(\frac{470}{950}\right)^{-\alpha_{wb}} - \left(\frac{470}{950}\right)^{-\alpha_{ff}}} \right] / b_{abs}(950nm) * BC \quad (5)$$

214
 215 Where two pairs of Ångström exponents values were utilized to obtain BC associated with fossil fuel (BC_{ff}) and wood
 216 burning (BC_{wb}). One of the largest sources of uncertainty in the aethalometer model is related to the section of α_{ff}
 217 and α_{wb} values (Healy et al., 2017; Zotter et al., 2017). In addition, the α_{ff} was typically in the range of ~ 0.8 —1.2 in
 218 ambient air whereas α_{wb} can vary from 1.6 to 2.2 (Saarikoski et al., 2021). However, we used the α_{ff} and α_{wb} values
 219 as 0.95 and 1.68 to calculate the BC source (Helin et al., 2018), since our measurement site is in a rural area and nearby
 220 a suburban area.

221 **3. RESULTS AND DISCUSSION**

222 **3.1. Overview of the field observations**

223 Figures S1 and S2 give an overview of the measurement location and the meteorological parameters, traces gases,
224 particle concentrations, and their optical properties during the campaign. The major wind directions at KIT Campus
225 Nord, 3 km east of the village of Eggenstein-Leopoldshafen, were northeast and southwest (Figure S1) caused by
226 channeling of the wind in the Rhine valley. The average wind speeds were 1.1 ± 0.8 (average \pm standard deviation) m
227 s^{-1} . Depending on meteorological conditions, local sources and regional transport had a major impact on air quality in
228 Leopoldshafen in summer (Shen et al., 2019). As shown in Figure S5, O_3 had diurnal variations with peaks at daytime
229 and an average of $41.3 \pm 26.2 \mu g m^{-3}$ during the campaign. In contrast, the relative humidity (RH) showed diurnal
230 variations with peaks at nighttime and an average of $68 \pm 16\%$ during the campaign (Figure S5). The average
231 temperature during the winter campaign was $6.5 \pm 5.6 \text{ }^\circ C$ and slowly increased from beginning to the end of the
232 campaign. NO_2 had high concentrations at some periods e.g. from 20th to 23rd February with $22 \pm 8.6 \mu g m^{-3}$ and
233 from 2nd to 4th March with $35 \pm 14 \mu g m^{-3}$. The average SO_2 concentration was $0.8 \pm 1.0 \mu g m^{-3}$, significantly lower than
234 the NO_2 concentrations. During some Saharan dust events, the $PM_{2.5}$ and PM_{10} mass concentrations were 21 ± 6 and
235 $45 \pm 20 \mu g m^{-3}$, respectively, from 18th to 26th February and 19 ± 6 and $24 \pm 7 \mu g m^{-3}$, respectively, from 1st to 4th March
236 as indicated by red boxes in the lowest panel of Figure S2. In addition, BC showed many spikes and a good correlation
237 ($r = 0.8$) with NO_2 (Figure S3). This indicates that there were many combustion events during the campaign (Figure
238 S3). The absorption Ångström exponents of particles between 370 and 520 nm ($AAE_{370-520}$) and $AAE_{660-950}$ had diurnal
239 variations with peaks at nighttime. We calculated the fraction of wood burning BC and fossil fuel BC as shown in
240 Figure S3 using the aAethalometer model (Sandradewi et al., 2008a). During the winter campaign, the biomass burning
241 BC was on average $0.61 \pm 0.049 \mu g m^{-3}$, mostly higher than $0.025 \pm 0.027 \mu g m^{-3}$ for fossil fuel BC. The $AAE_{370-520}$,
242 $AAE_{660-950}$, biomass burning BC, and NO_2 values were enhanced from 20th to 23rd February and 2nd to 4th March. This
243 indicates that strong biomass burning (BB) events were on these days. During this winter campaign, the BrC absorption
244 accounted for $\sim 40\%$ of total absorption caused by BC and BrC at 370 nm. This points to the at least regional or seasonal
245 importance of BrC absorption which has an important effect on air quality and climate.

246 **3.2. Mass concentrations and volatility of potential brown carbon molecules**

247 Figure 2 shows an overview of levoglucosan concentrations, BC concentrations, absorption of brown carbon at 370
248 nm (b_{brc370}), $AAE_{370-520}$, volatility, and mass concentrations of 178 potential brown carbon molecules identified in the

249 particle phase and 31 potential brown carbon molecules in the gas phase during the whole winter campaign. We
250 identified 178 potential BrC molecules according to the method developed by Lin et al., (2018) (cf. section 2.3.). The
251 mass of these molecules shows a good correlation ($r = 0.7 \pm 0.1$) with the absorption at 370 nm ($b_{\text{BrC}370}$) of BrC (sf.
252 Figure S6). This indicates that it is meaningful to extract these 178 potential BrC molecules from more than one
253 thousand and five hundred molecules detected by FIGAERO-CIMS based on the double bond equivalent/carbon
254 number ratio (DBE/C) of each molecule being higher than 0.5 and less than 0.9. The levoglucosan showed a good
255 correlation ($r = 0.7$) with BC. This is in line with the large fraction of biomass burning contributing to BC during the
256 winter campaign. Biomass burning BC accounted for $(71 \pm 40)\%$ of total BC as we discussed above. The 178 potential
257 BrC molecules detected in the particle phase correspond to an average mass concentrations of $83 \pm 44 \text{ ng m}^{-3}$. In
258 addition, the nitro aromatic compounds (NACs) were also detected during the winter campaign. The mass
259 concentrations of Σ NACs in the gas phase and particle phase were $1.9 \pm 1.5 \text{ ng m}^{-3}$ and $17.5 \pm 18.4 \text{ ng m}^{-3}$, respectively
260 (Tables S4 and S5). Mohr et al. (2013) found that five BrC molecules (nitro aromatic compounds) were 20 ng m^{-3}
261 detected by CIMS during winter in Detling, United Kingdom. Jiang et al. (2022) measured an average concentration
262 of five BrC molecules (nitro aromatic compounds) of $1.6 \pm 0.9 \text{ ng m}^{-3}$ during the winter at a kerbside in downtown
263 Karlsruhe, a city in southwest Germany and close to our measurement site. Therefore, the detection of the 178 potential
264 BrC molecules allows a more complete assessment of the BrC concentrations during this winter campaign. Their
265 concentrations were significantly higher for biomass burning (BB) events e.g., $144 \pm 41 \text{ ng m}^{-3}$ at BB event 1 and 124
266 $\pm 39 \text{ ng m}^{-3}$ at BB event 2, respectively. In addition, the absorption of brown carbon at 370 nm ($b_{\text{brC}370}$) had high peaks
267 with $\sim 100 \text{ Mm}^{-1}$ and the $\text{AAE}_{370-520}$ of particles increased from ~ 1.5 to ~ 2 during the BB events. The average
268 concentration of potential BrC in the gas phase was $8.5 \pm 6.7 \text{ ng m}^{-3}$ during the winter campaign. At BB events, their
269 concentration can reach up to 38 ng m^{-3} . Therefore, biomass burning had a significant impact on optical properties of
270 aerosol and brown carbon concentrations. The lowermost panel of Figure 2 shows the temporal variation of the average
271 volatility of brown carbon molecules in the gas and particle phase. The average volatility or saturation concentration
272 ($\log_{10}C_{\text{sat}}$) of potential BrC in the particle phase was ~~with~~ $-1.1 \pm 0.5 \mu\text{g m}^{-3}$ lower than $0.9 \pm 0.6 \mu\text{g m}^{-3}$ of potential BrC
273 in the gas phase during the winter campaign. Organic compounds with $\log_{10}C_{\text{sat}}$ lower than $-4.5 \mu\text{gm}^{-3}$, between -4.5
274 and $-0.5 \mu\text{gm}^{-3}$, between -0.5 and $2.5 \mu\text{gm}^{-3}$, and between 2.5 and $6.5 \mu\text{gm}^{-3}$ are termed extremely low-volatility
275 organic compounds (ELVOCs), low-volatility organic compounds (LVOCs), semi-volatile organic compounds
276 (SVOCs), and intermediate-volatility organic compounds (IVOCs), respectively (Donahue et al., 2009). Therefore,
277 BrC in the particle phase can be classified on average to the LVOCs and BrC in the gas phase to the SVOCs.

3.3 Absorption contribution of nitro aromatic compounds and potential brown carbon molecules

Black carbon dominated light absorption of aerosol particles with a contribution of 100% at 880 nm and decreasing to 73% at 370 nm. With shorter wavelengths, the brown carbon absorption contribution significantly increased contributing 27% of total aerosol absorption at 370 nm (Figure 3a). We have no independent quantification of the total organic aerosol mass loadings. However, we estimated the total organic mass as a fraction of $50 \pm 20\%$ of $PM_{2.5}$ which is a typical fraction for at the location (Song et al., 2022; Song et al., 2024). According to this assumption, the average organic mass concentration was $4.5 \pm 3.1 \mu\text{g m}^{-3}$. The organic mass detected by FIGAERO-CIMS based on calibrated sensitivity factors was $37 \pm 20\%$ of the estimated organic mass. This is in a similar range as observed in previous studies (Ye et al., 2021). We calculated the average light absorption of seven nitro aromatic compounds (NACs) by using the mass absorption coefficients (molecular MAC_{365} (Xie et al., 2017), given in Table S5 and the average concentrations measured, as shown in Table S5. Based on this, the mean light absorption of the sum of the seven NACs was calculated to be $0.2 \pm 0.2 \text{ Mm}^{-1}$. The absorption of the seven NACs contributed to $2.2 \pm 2.1\%$ of total BrC absorption at 370 nm (Figure 3b). contributing to $2.2 \pm 2.1\%$ of total BrC absorption at 370 nm, but they only contributed $0.45 \pm 0.32\%$ of the total organic mass.

In order to calculate the light absorption from the other 171 potential brown carbon molecules identified, we assumed an average MAC value of $9.5 \text{ m}^2 \text{ g}^{-1}$ at 370 nm for all BrC molecules to estimate their absorption (Jiang et al., 2022). So far, the MAC_{370} of most potential brown carbon molecules are still unknown. In addition, since the potential BrC molecules detected by FIGAERO-CIMS could have isomers effect, we did not calibrate mass absorption coefficients of 171 potential BrC. Despite these uncertainties, we think it is reasonable to estimate the order magnitude of the total BrC absorption based on this assumption. Based on this assumption, we calculated the light absorption of the 171 potential brown carbon molecules identified to $0.6 \pm 0.3 \text{ Mm}^{-1}$ at 370 nm as average for the whole winter campaign. This is half the values Jiang et al. (2022) found as mean light absorption of 316 potential BrC molecules of $1.2 \pm 0.2 \text{ Mm}^{-1}$ at 365 nm for downtown Karlsruhe in winter. Relative to this total organic aerosol particle mass and the measured brown carbon absorption, the 171 potential identified brown carbon molecules and 7 NACs only accounted for $2.6 \pm 1.5\%$ of the total organic mass, but explain $14 \pm 13\%$ of total brown carbon absorption at 370 nm (Figure 3b and 3c).

Palm et al. (2020) found that particulate nitroaromatic compounds (BrC molecules) can explain $29 \pm 15\%$ of average BrC light absorption at 405 nm, despite accounting for just $4 \pm 2\%$ of average OA mass in fresh wildfire plumes. Mohr et al. (2013) found that five nitroaromatic compounds (BrC molecules) are potentially important contributors to

306 absorption at 370 nm measured by an aethalometer and account for $4 \pm 2\%$ of UV light absorption by brown carbon in
307 Detling, United Kingdom during winter. Jiang et al. (2022) determined a mean light absorption of ~~the 316 potential~~
308 ~~BrC molecules~~ five nitro aromatic compounds -accounting for ~~$32 \pm 15\%$~~ $0.3 \pm 0.1\%$ of methanol-soluble BrC absorption
309 at 365 nm, but only accounted for ~~$2.5 \pm 0.6\%$~~ $0.03 \pm 0.01\%$ of the organic aerosol mass. Therefore, NACs are typical
310 brown carbon molecules with typically lower mass contributions to total organic aerosol but relatively higher
311 contributions to the total BrC absorption. ~~Therefore, even small mass fractions of strongly absorbing brown carbon~~
312 ~~molecules can dominate the brown carbon absorption.~~

313 3.4 Diurnal variations and sources of potential BrC in the gas phase

314 As shown in Figure 4a, the 31 gas-phase potential BrC (GBrC) molecules showed higher concentrations at daytime
315 (09:00-17:00) and lower concentrations between evening and early morning (18:00-08:00). Salvador et al. (2021) also
316 found that 16 gas-phase nitro-aromatic compounds (BrC molecules) measured by FIGAERO-CIMS were higher during
317 daytime and lower at nighttime during winter in rural China. As discussed above, strong biomass burning emissions
318 were mostly observed at evening and early morning hours. However, gas-phase BrC had no peaks during those time
319 periods. Therefore, the primary emission from biomass burning was not a major source for GBrC at KIT Campus Nord.
320 It seems to be mainly controlled by secondary formation (e.g., photochemical smog) or/and particle-to-gas partitioning
321 (Salvador et al., 2021).

322 To demonstrate how secondary formation and partitioning control the gas-phase BrC in rural Germany, we plotted
323 diurnal profiles of the average volatility and volatility fractions of IVOC, SVOC, and LVOC of the gas-phase BrC
324 (Figure 4b). The LVOC of BrC increased at evenings and decreased at daytime. In contrast, the IVOC of BrC increased
325 at daytime and reached $\sim 17\%$ of total $\log_{10}C^*$ (volatility) in gas-phase BrC while SVOC remained with a relative
326 constant fraction ($\sim 60\%$). Furthermore, the IVOC fraction of BrC in the particle-phase was only 1.5% with a flat
327 diurnal profile (Figure S7). The O/C ratio of gas-phase BrC also increased during daytime (Figure 4d). Therefore, the
328 higher fraction of IVOC in the gas phase at daytime is most likely caused by secondary formation e.g., photochemical
329 conversion/aging because of higher oxidant levels as indicated e.g., by higher concentration of ozone at same time
330 (Figure 4c) (Saarikoski et al., 2021). Figure S8 shows that BrC in the gas phase had a moderate positive correlation (r
331 $= 0.4$) with temperature. This explains why the temperature shows a similar diurnal profile as the gas-phase BrC.
332 Therefore, particle-to-gas partitioning was also an important source for gas-phase BrC. However, our results are not
333 consistent with previous studies where 16 BrC molecules in gas phase were mainly from primary emission during the

334 biomass burning evenings and secondary formation during the clear days in rural China (Salvador et al., 2021). Our
335 measurement site was several km away from biomass burning sites with ~7-10 km. And the 31 potential BrC in the
336 gas-phase sum up to $8.5 \pm 6.7 \text{ ng m}^{-3}$, significantly lower than 1720 ng m^{-3} of 16 BrC (Salvador et al., 2021). Cheng
337 et al. (2021) found that secondary formation was a strong source for five BrC molecules in the gas-phase. Therefore,
338 BrC in the gas-phase are less influenced ~~by~~ primary emissions from biomass burning but are mainly controlled
339 by secondary formation and partitioning in rural Germany.

340 3.5 Diurnal variations and sources of potential BrC in the particle phase

341 The 178 potential BrC molecules in the particle phase (PBrC) exhibited two peaks in the diurnal profile (Figure 4a)
342 averaged over the whole winter campaign. They increased from 19:00 to 01:00 with a peak at $82 \pm 35 \text{ ng m}^{-3}$ around
343 midnight. Then the PBrC slowly decreased after midnight. However, they increased again from 6:00 to 08:00 and
344 forming a second peak with $102 \pm 49 \text{ ng m}^{-3}$ in the morning. During daytime, they decreased reaching the lowest values
345 with $61 \pm 31 \text{ ng m}^{-3}$ at 14:00-15:00. During the nighttime and morning hours, the higher mass concentrations of PBrC
346 were caused by residential wood burning emissions. Consistently, higher PM_{2.5} concentration levels at nighttime at a
347 rural site near Karlsruhe, Germany, could be assigned to wood burning emissions from wood stove operation during
348 winter (Thieringer et al., 2022). The low mass concentrations of PBrC at daytime could be explained by photobleaching
349 and evaporation of BrC, and/or dilution by the increasing planetary boundary layer heights (Satish et al., 2017). Satish
350 et al. (2017) found that BrC over the Indo-Gangetic Plain had two peaks of BrC at evening and morning hours, and
351 lowest values during daytime.

352 To determine the sources of brown carbon, we used the edge approach (Day et al., 2015). It allows to estimate the
353 contribution of primary biomass burning (BB) to the measured BrC concentrations using levoglucosan as a primary
354 source tracer. This approach is analogous to the widely used elemental carbon (EC) tracer approach, in which EC is
355 used to distinguish the primary organic carbon (POC) and secondary organic carbon (SOC) in total organic carbon
356 (OC) measurements (Day et al., 2015; Cabada et al., 2004). Levoglucosan (lev) and potential BrC were measured
357 online by the same instruments and under the same conditions. As discussed above, we observed a good correlation (r
358 = 0.8) between levoglucosan and BC during the winter campaign. Therefore, levoglucosan is a suitable tracer for
359 primary BB. Please note that we did not calibrate the sensitivities of levoglucosan detected by FIGAERO-CIMS.
360 Therefore, it could cause some uncertainties to estimate brown carbon from biomass burning and secondary formation.
361 Figure 5a shows that the blue points can be used as edge points to determine the ratio of BrC/levoglucosan at the

362 primary emissions from biomass burning. The relative contributions of primary emissions (BB) and secondary (sec)
363 formation for total BrC molecules were estimated using the following expression:

$$364 \quad BrC_{BB} = \left(\frac{[BrC]}{[lev]_{BB}} \right) * [lev.]$$

$$365 \quad [BrC_{sec}] = [BrC_{Tot}] - [BrC_{BB}]$$

366 Where $([BrC]/[lev])_{BB}$ is the ratio of the concentration of the BrC to that of levoglucosan in the primary emissions from
367 biomass burning and this value is 1.1 ± 0.1 (Figure 5a), BrC_{BB} and BrC_{sec} are the fractions of BrC generated through
368 biomass burning and secondary production, respectively. BrC_{Tot} and $lev.$ are the measured concentrations of BrC and
369 levoglucosan during the winter campaign. Using this approach, we calculated the diurnal profiles of BrC from primary
370 emissions (BrC_{BB}) and secondary formation (BrC_{sec}) shown in Figure 5b. The uncertainty of the splitting between BrC
371 from biomass burning and of secondary origin is mainly based on the levoglucosan concentration for which we have
372 included the calibration. Based on this we estimated the uncertainty of the BrC source splitting to $\pm 35\%$. The mass
373 fraction of BrC_{sec} increased at daytime and decreased at evening. This indicates that the secondary formation for BrC
374 in the particle phase was enhanced during daytime, facilitated by the higher levels of oxidants e.g. O_3 (Figure 4c). The
375 mass fraction of BrC_{BB} had two peaks at early morning and in the evening hours, respectively. This may be caused by
376 residential wood burning emissions. BrC_{BB} accounts for $39 \pm 21\%$ of the total BrC as averaged for the whole
377 measurement period. During biomass burning events, the BrC_{BB} is a major mass fraction for total BrC that accounts
378 for $61 \pm 13\%$ during BB-event1 and $65 \pm 12\%$ during BB-event-2, respectively. Therefore, the primary emissions of
379 BrC have a significant impact on BrC, especially, at biomass burning events. However, on average over the whole
380 campaign, BrC_{sec} dominates the mass fraction of BrC with $61 \pm 21\%$. Therefore, the secondary formation can be
381 considered as an important source for BrC in rural Germany. Consistently, secondary formation from biomass burning
382 emission is important for the brown carbon absorption in the Switzerland, the central Europe. (Moschos et al., 2018).
383 Secondary sources for BrC were more important for absorption than primary ones in the Southeastern Margin of the
384 Tibetan Plateau (Wang et al., 2019b).

385 To further investigate the oxidation of BrC in the particle phase we plotted, the diurnal profiles of O/C ratios of BrC
386 during the whole campaign was measured, as shown in Figure 6. The O/C ratio of the potential BrC molecules increased
387 during daytime and decreased at nighttime. This is an indication for an impact of photo-oxidation on BrC either during
388 formation or aging leading to an increase of its O/C ratio. Consequently, the O/C ratio of the potential BrC molecules

389 shows a positive correlation ($r = 0.8$) with ozone, another product of photo chemistry. In contrast, the light absorption
390 of BrC at 370 nm ($b_{\text{brc}370}$) and the double bond equivalent (DBE) decreased at daytime and increased at nighttime.
391 During daytime, the absorption of brown carbon at 370 nm decreased due to lower DBE and higher O/C values of
392 brown carbon caused by photooxidation. This is in accordance with previous studies where atmospheric photooxidation
393 diminishes light absorption of primary brown carbon aerosol from biomass burning (Sumlin et al., 2017). Oxidative
394 whitening can reduce light absorption of brown carbon during the day (Hems et al., 2021).

395 **Conclusions**

396 The chemical composition, diurnal variation, and sources of brown carbon aerosol were investigated during February-
397 March 2021 in a rural area, at KIT Campus Nord, a location characteristic for central Europe. The 178 potential brown
398 carbon molecules (including 7 nitro aromatic compounds, NACs) identified in the particle phase contributed on average
399 $83 \pm 44 \text{ ng m}^{-3}$ and 31 potential brown carbon molecules (including 4 NACs) identified in the gas phase contributed
400 on average $8.5 \pm 6.7 \text{ ng m}^{-3}$ during the whole campaign. During dedicated biomass burning events, potential BrC
401 concentrations in the particle phase were significantly higher with up to $\sim 254 \text{ ng m}^{-3}$. The average light absorption of
402 seven NACs in the particle phase was $0.2 \pm 0.2 \text{ Mm}^{-1}$, contributing to $2.2 \pm 2.1\%$ of total BrC absorption at 370 nm. The
403 178 identified potential brown carbon molecules only accounted for $2.6 \pm 1.5\%$ of the total organic mass, but explained
404 $14 \pm 13\%$ of the total brown carbon absorption at 370 nm, assuming a MAC_{370} as $9.5 \text{ m}^2 \text{ g}^{-1}$. This shows that NACs
405 are important molecules for brown carbon, a small fraction of the brown carbon molecules dominates the overall
406 absorption. This indicates the great importance of identifying these molecules, the strong absorbers, to predict aerosol
407 absorption.

408 Diurnal variations show that the particle-phase potential BrC had two peaks at early morning and evening hours,
409 respectively. These were mainly caused by residential wood burning emissions. In contrast, the gas-phase potential
410 BrC showed higher concentrations at daytime and lower concentrations at nighttime. The gas-phase BrC molecules
411 were mainly controlled by secondary formation (e.g. by photochemical processes) and particle-to-gas partitioning.
412 The two main sources contributed to particle-phase BrC were primary emission from biomass burning and secondary
413 formation. Secondary formation, e.g. by photooxidation, is an important source of particle-phase BrC corresponding
414 to increasing O/C ratios of BrC during daytime and a positive correlation ($r = 0.8$) with ozone concentrations. In
415 addition, the DBE of the particle-phase decreased during daytime. This indicates that the absorption of brown carbon

416 at 370 nm decreased due to lower DBE and a higher O/C ratio due to the photooxidation of brown carbon. Compared
417 with previous measurements in central Europe (Lukács et al., 2007; Zhang et al., 2020), our study found that secondary
418 formation, e.g., photochemical processes, was an important source for BrC in gas and particle phases. To improve air
419 quality in winter, we need to reduce biomass burning emissions (e.g., regulate wood stoves) but also reduce the
420 precursors to form secondary aerosol. Overall, this study provides good insight into the light absorption, sources, and
421 diurnal variation from real-time observations of brown carbon molecules in central Europe by using mass spectrometry
422 and an aethalometer.

423 **Data availability**

424 ~~Data are available upon request to the corresponding author.~~The data related to this article are accessible at KIT open
425 data (<https://doi.org/10.35097/d0prpzxqkq2t09y>, Jiang et al., 2024).

426 **Competing interests**

427 At least one of the (co-)authors is a member of the editorial board of Atmospheric Chemistry and Physics.

428 **Author contributions**

429 FJ and HS designed the measurement campaign. FJ, LG, JS, and HS performed the experimental work. FJ did
430 FIGAERO-CIMS and AE33 data analysis. HS and HZ processed the trace gas and meteorological data, respectively.
431 UE did CIMS sensitivity calibrations. TL gave general comments for this paper. FJ wrote the paper with contributions
432 from all co-authors.

433 **ACKNOWLEDGMENTS**

434 The authors gratefully thank the staff of IMK-AAF for providing substantial technical support during the field
435 campaigns under COVID conditions. Furthermore, Feng Jiang and Junwei Song are thankful for the support from the
436 China Scholarship Council (CSC).

437

438 REFERENCES

439 Andreae, M. O., and Gelencser, A.: Black carbon or brown carbon? The nature of light-absorbing carbonaceous
440 aerosols, *Atmos. Chem. Phys.*, 6, 3131-3148, <https://doi.org/10.5194/acp-6-3131-2006>, 2006.

441 Cabada, J. C., Pandis, S. N., Subramanian, R., Robinson, A. L., Polidori, A., and Turpin, B.: Estimating the secondary
442 organic aerosol contribution to PM_{2.5} using the EC tracer method, *Aerosol Sci. Technol.*, 38, 140-155,
443 <https://doi.org/10.1080/02786820390229084>, 2004.

444 Chen, Q. C., Chen, Q., Hua, X. Y., Guan, D. J., and Chang, T.: Gas-phase brown carbon: Absorbance and chromophore
445 types, *Atmos. Environ.*, 264, 118646, <https://doi.org/10.1016/j.atmosenv.2021>, 2021.

446 Cheng, X., Chen, Q., Li, Y., Huang, G., Liu, Y., Lu, S., Zheng, Y., Qiu, W., Lu, K., Qiu, X., Bianchi, F., Yan, C.,
447 Yuan, B., Shao, M., Wang, Z., Canagaratna, M. R., Zhu, T., Wu, Y., and Zeng, L.: Secondary Production of Gaseous
448 Nitrated Phenols in Polluted Urban Environments, *Environ. Sci. Technol.*, 55, 4410-4419,
449 <https://doi.org/10.1021/acs.est.0c07988>, 2021.

450 Daumit, K. E., Kessler, S. H., and Kroll, J. H.: Average chemical properties and potential formation pathways of highly
451 oxidized organic aerosol, *Farad. Disc.*, 165, 181-202, <https://doi.org/10.1039/c3fd00045a>, 2013.

452 Day, M. C., Zhang, M. H., and Pandis, S. N.: Evaluation of the ability of the EC tracer method to estimate secondary
453 organic carbon, *Atmos. Environ.*, 112, 317-325, <https://doi.org/10.1016/j.atmosenv.2015.04.044>, 2015.

454 Donahue, N. M., Robinson, A. L., and Pandis, S. N.: Atmospheric organic particulate matter: From smoke to secondary
455 organic aerosol, *Atmos. Environ.*, 43, 94-106, <https://doi.org/10.1016/j.atmosenv.2008.09.055>, 2009.

456 Drinovec, L., Mocnik, G., Zotter, P., Prevot, A. S. H., Ruckstuhl, C., Coz, E., Rupakheti, M., Sciare, J., Muller, T.,
457 Wiedensohler, A., and Hansen, A. D. A.: The "dual-spot" Aethalometer: an improved measurement of aerosol black
458 carbon with real-time loading compensation, *Atmos. Meas. Tech.*, 8, 1965-1979, <https://doi.org/10.5194/amt-8-1965-2015>,
459 2015, 2015.

460 Jing, D., Huang, R., Lin, C., Shen, J., Yang, L., Yuan, W., Wang, Y., Liu, Y., and Xu W.: Aromatic Nitration Enhances
461 Absorption of Biomass Burning Brown Carbon in an Oxidizing Urban Environment, *Environ. Sci. Technol.*, 58, 17344-
462 54, <https://doi.org/10.1021/acs.est.4c05558>, 2024.

463 ~~Drinovec, L., G. Mocnik, P. Zotter, A. S. H. Prevot, C. Ruckstuhl, E. Coz, M. Rupakheti, J. Sciare, T. Muller, A.~~
464 ~~Wiedensohler, and A. D. A. Hansen.: The "dual spot" Aethalometer: an improved measurement of aerosol black carbon~~
465 ~~with real time loading compensation, Atmos. Meas. Tech., 8, 1965-79, https://doi.org/10.5194/amt-8-1965-2015, 2015.~~

466 Gundel, L. A., Dod, R. L., Rosen, H., and Novakov, T.: The relationship between optical attenuation and black carbon
467 concentration for ambient and source particles, *Sci. Total Environ.*, 36, 197-202, [https://doi.org/10.1016/0048-](https://doi.org/10.1016/0048-9697(84)90266-3)
468 9697(84)90266-3, 1984.

469 Healy, R. M., U. Sofowote, Y. Su, J. Deboz, M. Noble, C. H. Jeong, J. M. Wang, N. Hilker, G. J. Evans, G. Doerksen,
470 K. Jones, and A. Munoz.: Ambient measurements and source apportionment of fossil fuel and biomass burning black
471 carbon in Ontario, *Atmos. Environ.*, 161, 34-47, <https://doi.org/10.1016/j.atmosenv.2017.04.034>, 2017.

472 Helin, A., Niemi, J. V., Virkkula, A., Pirjola, L., Teinilä, K., Backman, J., Aurela, M., Saarikoski, S., Rönkkö, T.,
473 Asmi, E., and Timonen, H.: Characteristics and source apportionment of black carbon in the Helsinki metropolitan
474 area, Finland, *Atmos. Environ.*, 190, 87-98, <https://doi.org/10.1016/j.atmosenv.2018.07.022>, 2018.

475 Hems, R. F., Schnitzler, E. G., Liu-Kang, C., Cappa, C. D., and Abbatt, J. P. D.: Aging of Atmospheric Brown Carbon
476 Aerosol, *ACS Earth Space Chem.*, 5, 722-748, <https://doi.org/10.1021/acsearthspacechem.0c00346>, 2021.

477 Huang, R.-J., Yang, L., Cao, J., Chen, Y., Chen, Q., Li, Y., Duan, J., Zhu, C., Dai, W., Wang, K., Lin, C., Ni, H.,
478 Corbin, J. C., Wu, Y., Zhang, R., Tie, X., Hoffmann, T., O'Dowd, C., and Dusek, U.: Brown Carbon Aerosol in Urban
479 Xi'an, Northwest China: The Composition and Light Absorption Properties, *Environ. Sci. Technol.*, 52, 6825-6833,
480 <https://doi.org/10.1021/acs.est.8b02386>, 2018.

481 Huang, W., Saathoff, H., Pajunoja, A., Shen, X., Naumann, K.H., Wagner, R., Virtanen, A., Leisner, T., and Mohr, C.:
482 alpha-Pinene secondary organic aerosol at low temperature: chemical composition and implications for particle
483 viscosity, *Atmos. Chem. Phys.*, 18, 2883-98, <https://doi.org/10.5194/acp-18-2883-2018>, 2018.

484 Huang, W., Saathoff, H., Shen, X., Ramisetty, R., Leisner, T., and Mohr, C.: Chemical Characterization of Highly
485 Functionalized Organonitrates Contributing to Night-Time Organic Aerosol Mass Loadings and Particle Growth,
486 *Environ. Sci. Technol.*, 53, 1165-1174, <https://doi.org/10.1021/acs.est.8b05826>, 2019.

487 ~~Huang, W., Saathoff, H., Shen, X. L., Ramisetty, R., Leisner, T., and Mohr, C.: Seasonal characteristics of organic~~
488 ~~aerosol chemical composition and volatility in Stuttgart, Germany, *Atmos. Chem. Phys.* 19, 11687-11700,~~
489 ~~<https://doi.org/10.5194/acp-19-11687-2019>, 2019b.~~

490 Jiang, F., Song, J. W., Bauer, J., Gao, L. Y., Vallon, M., Gebhardt, R., Leisner, T., Norra, S., and Saathoff, H.:
491 Chromophores and chemical composition of brown carbon characterized at an urban kerbside by excitation-emission
492 spectroscopy and mass spectrometry, *Atmos. Chem. Phys.*, 22, 14971-14986, [https://doi.org/10.5194/acp-22-14971-](https://doi.org/10.5194/acp-22-14971-2022)
493 [2022](https://doi.org/10.5194/acp-22-14971-2022), 2022.

494 Jiang, F., Siemens, K., Linke, C., Li, Y., Gong, Y., Leisner, T., Laskin, A., and Saathoff, H.: Molecular analysis of
495 secondary organic aerosol and brown carbon from the oxidation of indole. *Atmos. Chem. Phys.*, 24(4), 2639-2649.
496 <https://doi.org/10.5194/acp-24-2639-2024>, 2024.

497 ~~Jiang, F., Saathoff, H., Ezenobi, U., Song, J., Zhang, H., Gao, L., and Leisner, T.: Dataset for the publication: Brown~~
498 ~~carbon aerosol in rural Germany: sources, chemistry, and diurnal variations, Karlsruhe Institute of Technology [data~~
499 ~~set], <https://doi.org/10.35097/d0prpzxqkq2t09y>, 2024.~~

500 Lack, D. A., and Langridge, J. M.: On the attribution of black and brown carbon light absorption using the Ångström
501 exponent. *Atmos. Chem. Phys.*, 13, 10535-43, <https://doi.org/10.5194/acp-13-10535-2013>, 2013.

502 Laskin, A., Laskin, J., and Nizkorodov, S. A.: Chemistry of Atmospheric Brown Carbon, *Chem. Rev.*, 115, 4335-4382,
503 <https://doi.org/10.1021/cr5006167>, 2015.

504 Lee, B., Lopez-Hilfiker, F. D., D'Ambro, E. L., Zhou, P. T., Boy, M., Petaja, T., Hao, L. Q., Virtanen, A., and Thornton,
505 J. A.: Semi-volatile and highly oxygenated gaseous and particulate organic compounds observed above a boreal forest
506 canopy, *Atmos. Chem. Phys.*, 11547-11562, <https://doi.org/10.5194/acp-18-11547-2018>, 2018.

507 Lin, P., Liu, J., Shilling, J. E., Kathmann, S. M., Laskin, J., and Laskin, A.: Molecular characterization of brown carbon
508 (BrC) chromophores in secondary organic aerosol generated from photo-oxidation of toluene, *Phys. Chem. Chem.*
509 *Phys.*, 17, 23312-23325, <https://doi.org/10.1039/c5cp02563j>, 2015.

510 Lin, P., Aiona, P. K., Li, Y., Shiraiwa, M., Laskin, J., Nizkorodov, S. A., and Laskin, A.: Molecular Characterization
511 of Brown Carbon in Biomass Burning Aerosol Particles, *Environ. Sci. Technol.*, 50, 11815-24,
512 <https://doi.org/10.1021/acs.est.6b03024>, 2016.

513 Lin, P., Fleming, L. T., Nizkorodov, S. A., Laskin, J., and Laskin, A.: Comprehensive Molecular Characterization of
514 Atmospheric Brown Carbon by High Resolution Mass Spectrometry with Electrospray and Atmospheric Pressure
515 Photoionization, *Anal. Chem.*, 90, 12493-502, <https://doi.org/10.1021/acs.analchem.8b02177>, 2018.

516 Linke, C., Ibrahim, I., Schleicher, N., Hitzenberger, R., Andreae, M. O., Leisner, T., and Schnaiter, M.: A novel single-
517 cavity three-wavelength photoacoustic spectrometer for atmospheric aerosol research, *Atmos. Meas. Tech.*, 9, 5331-
518 46, <https://doi.org/10.5194/amt-9-5331-2016>, 2016.

519 Liu, X., Wang, H., Wang, F., Lv, S., Wu, C., Zhao, Y., Zhang, S., Liu, S., Xu, X., Lei, Y., and Wang, G.: Secondary
520 Formation of Atmospheric Brown Carbon in China Haze: Implication for an Enhancing Role of Ammonia, *Environ.*
521 *Sci. Technol.*, 57, 11163-11172, <https://doi.org/10.1021/acs.est.3c03948>, 2023.

522 Lukács, H., Gelencsér, A., Hammer, S., Puxbaum, H., Pio, C., Legrand, M., Kasper-Giebl, A., Handler, M., Limbeck,
523 A., Simpson, D., and Preunkert, S.: Seasonal trends and possible sources of brown carbon based on 2-year aerosol
524 measurements at six sites in Europe, *J. Geophys. Res.*, 112, <https://doi.org/10.1029/2006JD008151>, 2007.

525 Lopez-Hilfiker, F. D., Mohr, C., Ehn, M., Rubach, F., Kleist, E., Wildt, J., Mentel, T. F., Lutz, A., Hallquist, M.,
526 Worsnop, D., and Thornton, J. A.: A novel method for online analysis of gas and particle composition: description and
527 evaluation of a Filter Inlet for Gases and AEROSols (FIGAERO), *Atmos. Meas. Tech.*, 7, 983-1001,
528 <https://doi.org/10.5194/amt-7-983-2014>, 2014.

529 Lopez-Hilfiker, F. D., Iyer, S., Mohr, C., Lee, B. H., D'Ambro, E. L., Kurten, T., and Thornton, J. A.: Constraining the
530 sensitivity of iodide adduct chemical ionization mass spectrometry to multifunctional organic molecules using the

531 collision limit and thermodynamic stability of iodide ion adducts, *Atmos. Meas. Tech.*, 9, 1505-12,
532 <https://doi.org/10.5194/amt-9-1505-2016>, 2016.

533 Mohr, C., Lopez-Hilfiker, F. D., Zotter, P., Prevot, A. S. H., Xu, L., Ng, N. L., Herndon, S. C., Williams, L. R., Franklin,
534 J. P., Zahniser, M. S., Worsnop, D. R., Knighton, W. B., Aiken, A. C., Gorkowski, K. J., Dubey, M. K., Allan, J. D.,
535 and Thornton, J. A.: Contribution of Nitrated Phenols to Wood Burning Brown Carbon Light Absorption in Detling,
536 United Kingdom during Winter Time, *Environ. Sci. Technol.*, 47, 6316-6324, <https://doi.org/10.1021/es400683v>, 2013.

537 Moise, T., Flores, J. M., and Rudich, Y.: Optical Properties of Secondary Organic Aerosols and Their Changes by
538 Chemical Processes, *Chem. Rev.*, 115, 4400-4439, <https://doi.org/10.1021/cr5005259>, 2015.

539 Montoya-Aguilera, J., Horne, J. R., Hinks, M. L., Fleming, L. T., Perraud, V., Lin, P., Laskin, A., Laskin, J., Dabdub,
540 D., and Nizkorodov, S. A.: Secondary organic aerosol from atmospheric photooxidation of indole, *Atmos. Chem. Phys.*,
541 17, 11605-11621, <https://doi.org/10.5194/acp-17-11605-2017>, 2017.

542 Moschos, V., Kumar, N. K., Daellenbach, K. R., Baltensperger, U., Prevot, A. S. H., and El Haddad, I.: Source
543 Apportionment of Brown Carbon Absorption by Coupling Ultraviolet-Visible Spectroscopy with Aerosol Mass
544 Spectrometry, *Environ. Sci. Tech. Lett.*, 5, 302-308, <https://doi.org/10.1021/acs.estlett.8b00118>, 2018.

545 Moschos, V., Gysel-Beer, M., Modini, R. L., Corbin, J. C., Massabo, D., Costa, C., Danelli, S. G., Vlachou, A.,
546 Daellenbach, K. R., Szidat, S., Prati, P., Prevot, A. S. H., Baltensperger, U., and El Haddad, I.: Source-specific light
547 absorption by carbonaceous components in the complex aerosol matrix from yearly filter-based measurements, *Atmos.*
548 *Chem. Phys.*, 21, 12809-12833, <https://doi.org/10.5194/acp-21-12809-2021>, 2021.

549 Palm, B. B., Peng, Q. Y., Fredrickson, C. D., Lee, B., Garofalo, L. A., Pothier, M. A., Kreidenweis, S. M., Farmer, D.
550 K., Pokhrel, R. P., Shen, Y. J., Murphy, S. M., Permar, W., Hu, L., Campos, T. L., Hall, S. R., Ullmann, K., Zhang,
551 X., Flocke, F., Fischer, E. V., and Thornton, J. A.: Quantification of organic aerosol and brown carbon evolution in
552 fresh wildfire plumes, *P. Natl. Acad. Sci. USA.*, 117, 29469-29477, <https://doi.org/10.1073/pnas.2012218117>, 2020.

553 Park, R. J., Kim, M. J., Jeong, J. I., Youn, D., and Kim, S.: A contribution of brown carbon aerosol to the aerosol light
554 absorption and its radiative forcing in East Asia, *Atmos. Environ.*, 44, 1414-1421,
555 <https://doi.org/10.1016/j.atmosenv.2010.01.042>, 2010.

556 Saarikoski, S., Niemi, J. V., Aurela, M., Pirjola, L., Kousa, A., Ronkko, T., and Timonen, H.: Sources of black carbon
557 at residential and traffic environments obtained by two source apportionment methods, *Atmos. Chem. Phys.*, 21,
558 14851-14869, <https://doi.org/10.5194/acp-21-14851-2021>, 2021.

559 Saathoff, H., Naumann, K. H., Schnaiter, M., Schöck, W., Möhler, O., Schurath, U., Weingartner, E., Gysel, M., and
560 Baltensperger, U.: Coating of soot and (NH₄)₂SO₄ particles by ozonolysis products of α -pinene, *J. Aerosol Sci.*, 34,
561 1297-321, [https://doi.org/10.1016/S0021-8502\(03\)00364-1](https://doi.org/10.1016/S0021-8502(03)00364-1), 2003.

562 Salvador, C. M. G., Tang, R. Z., Priestley, M., Li, L. J., Tsiligiannis, E., Le Breton, M., Zhu, W. F., Zeng, L. M., Wang,
563 H., Yu, Y., Hu, M., Guo, S., and Hallquist, M.: Ambient nitro-aromatic compounds - biomass burning versus secondary
564 formation in rural China, *Atmos. Chem. Phys.*, 21, 1389-1406, <https://doi.org/10.5194/acp-21-1389-2021>, 2021.

565 Sandradewi, J., Prevot, A. S. H., Szidat, S., Perron, N., Alfarra, M. R., Lanz, V. A., Weingartner, E., and Baltensperger,
566 U.: Using aerosol light absorption measurements for the quantitative determination of wood burning and traffic
567 emission contributions to particulate matter, *Environ. Sci. Technol.*, 42, 3316-3323,
568 <https://doi.org/10.1021/es702253m>, 2008a.

569 Sandradewi, J., Prevot, A. S. H., Weingartner, E., Schmidhauser, R., Gysel, M., and Baltensperger, U.: A study of
570 wood burning and traffic aerosols in an Alpine valley using a multi-wavelength Aethalometer, *Atmos. Environ.*, 42,
571 101-112, <https://doi.org/10.1016/j.atmosenv.2007.09.034>, 2008b.

572 Satish, R., Shamjad, P., Thamban, N., Tripathi, S., and Rastogi, N.: Temporal Characteristics of Brown Carbon over
573 the Central Indo-Gangetic Plain, *Environ. Sci. Technol.*, 51, 6765-6772, <https://doi.org/10.1021/acs.est.7b00734>, 2017.

574 Shen, X. L., Vogel, H., Vogel, B., Huang, W., Mohr, C., Ramisetty, R., Leisner, T., Prévôt, A. S. H., and Saathoff, H.:
575 Composition and origin of PM_{2.5} aerosol particles in the upper Rhine valley in summer. *Atmos. Chem. Phys.*, 19,
576 13189-13208. <https://doi.org/10.5194/acp-19-13189-2019>, 2019.

577 Siemens, K., Morales, A., He, Q., Li, C., Hettiyadura, A. P. S., Rudich, Y., and Laskin, A.: Molecular Analysis of
578 Secondary Brown Carbon Produced from the Photooxidation of Naphthalene, *Environ. Sci. Technol.*, 56, 3340-3353,
579 <https://doi.org/10.1021/acs.est.1c03135>, 2022.

580 ~~Song, J., H. Saathoff, F. Jiang, L. Gao, H. Zhang, and T. Leisner.: Sources of organic gases and aerosol particles and~~
581 ~~their roles in nighttime particle growth at a rural forested site in southwest Germany, *Atmos. Chem. Phys.*, 24, 6699-~~
582 ~~717, <https://doi.org/10.5194/acp-24-6699-2024>, 2024.~~ Song, J. W., Saathoff, H., Gao, L. Y., Gebhardt, R., Jiang, F.,
583 ~~Vallon, M., Bauer, J., Norra, S., and Leisner, T.: Variations of PM_{2.5} sources in the context of meteorology and~~
584 ~~seasonality at an urban street canyon in Southwest Germany, *Atmos. Environ.* 282,~~
585 ~~<https://doi.org/10.1016/j.atmosenv.2022.119147>, 2022.~~

586 Sumlin, B. J., Pandey, A., Walker, M. J., Pattison, R. S., Williams, B. J., and Chakrabarty, R. K.: Atmospheric
587 Photooxidation Diminishes Light Absorption by Primary Brown Carbon Aerosol from Biomass Burning, *Environ. Sci.*
588 *Technol. Lett.*, 4, 540-545, <https://doi.org/10.1021/acs.estlett.7b00393>, 2017.

589 Tang, J., Li, J., Su, T., Han, Y., Mo, Y. Z., Jiang, H. X., Cui, M., Jiang, B., Chen, Y. J., Tang, J. H., Song, J. Z., Peng,
590 P. A., and Zhang, G.: Molecular compositions and optical properties of dissolved brown carbon in biomass burning,
591 coal combustion, and vehicle emission aerosols illuminated by excitation-emission matrix spectroscopy and Fourier
592 transform ion cyclotron resonance mass spectrometry analysis, *Atmos. Chem. Phys.*, 20, 2513-2532,
593 <https://doi.org/10.5194/acp-20-2513-2020>, 2020.

594 Teich, M., van Pinxteren, D., Kecorius, S., Wang, Z. B., and Herrmann, H.: First Quantification of Imidazoles in
595 Ambient Aerosol Particles: Potential Photosensitizers, Brown Carbon Constituents, and Hazardous Components,
596 *Environ. Sci. Technol.*, 50, 1166-1173, <https://doi.org/10.1021/acs.est.5b05474>, 2016.

597 Teich, M., van Pinxteren, D., Wang, M., Kecorius, S., Wang, Z. B., Muller, T., Mocnik, G., and Herrmann, H.:
598 Contributions of nitrated aromatic compounds to the light absorption of water-soluble and particulate brown carbon in
599 different atmospheric environments in Germany and China, *Atmos. Chem. Phys.*, 17, 1653-1672,
600 <https://doi.org/10.5194/acp-17-1653-2017>, 2017.

601 Thieringer, J. R. D., Szabadi, J., Meyer, J., and Dittler, A.: Impact of Residential Real-World Wood Stove Operation
602 on Air Quality concerning PM2.5 Immission, Processes, 10, 545, <https://doi.org/10.3390/pr10030545>, 2022.

603 ~~Thompson, S. L., Yatavelli, R. L. N., Stark, H., Kimmel, J. R., Krechmer, J. E., Day, D. A., Hu, W., Isaacman-~~
604 ~~VanWertz, G., Yee, L., Goldstein, A. H., Khan, M. A. H., Holzinger, R., Kreisberg, N., Lopez-Hilfiker, F. D., Mohr,~~
605 ~~C., Thornton, J. A., Jayne, J. T., Canagaratna, M., Worsnop, D. R., and Jimenez, J. L.: Field intercomparison of the~~
606 ~~gas/particle partitioning of oxygenated organics during the Southern Oxidant and Aerosol Study (SOAS) in 2013,~~
607 ~~*Aerosol Sci. Technol.* 51, 30-56, <https://doi.org/10.1080/02786826.2016.1254719>, 2017.~~

608 Wang, Q., Ye, J., Wang, Y., Zhang, T., Ran, W., Wu, Y., Tian, J., Li, L., Zhou, Y., Hang Ho, S. S., Dang, B., Zhang,
609 Q., Zhang, R., Chen, Y., Zhu, C., and Cao, J.: Wintertime Optical Properties of Primary and Secondary Brown Carbon
610 at a Regional Site in the North China Plain, *Environ. Sci. Technol.*, 53, 12389-12397,
611 <https://doi.org/10.1021/acs.est.9b03406>, 2019a.

612 Wang, Q. Y., Han, Y. M., Ye, J. H., Liu, S. X., Pongpiachan, S., Zhang, N. N., Han, Y. M., Tian, J., Wu, C., Long, X.,
613 Zhang, Q., Zhang, W. Y., Zhao, Z. Z., and Cao, J. J.: High Contribution of Secondary Brown Carbon to Aerosol Light
614 Absorption in the Southeastern Margin of Tibetan Plateau, *Geophys. Res. Lett.*, 46, 4962-4970,
615 <https://doi.org/10.1029/2019gl082731>, 2019b.

616 Wu, G., Wan, X., Gao, S., Fu, P., Yin, Y., Li, G., Zhang, G., Kang, S., Ram, K., and Cong, Z.: Humic-like substances
617 (HULIS) in aerosols of central Tibetan Plateau (Nam Co, 4730 m asl): Abundance, light absorption properties and
618 sources, *Environ. Sci. Technol.*, 52, 7203-7211, <https://doi.org/10.1021/acs.est.8b01251>, 2018.

619 Xie, M., Chen, X., Hays, M. D., Lewandowski, M., Offenberg, J., Kleindienst, T. E., and Holder, A. L.: Light
620 Absorption of Secondary Organic Aerosol: Composition and Contribution of Nitroaromatic Compounds, *Environ. Sci.*
621 *Technol.*, 51, 11607-11616, <https://doi.org/10.1021/acs.est.7b03263>, 2017.

622 Xu, J. Z., Hettiyadura, A. P. S., Liu, Y. M., Zhang, X. H., Kang, S. C., and Laskin, A.: Regional Differences of
623 Chemical Composition and Optical Properties of Aerosols in the Tibetan Plateau, *J. Geophys. Res.-Atmos.*, 125,
624 e2019JD031226, <https://doi.org/10.1029/2019jd031226>, 2020.

625 Yang, Z., Tsona, N. T., George, C., and Du, L.: Nitrogen-Containing Compounds Enhance Light Absorption of
626 Aromatic-Derived Brown Carbon, *Environ. Sci. Technol.*, 56, 4005-4016, <https://doi.org/10.1021/acs.est.1c08794>,
627 2022.

628 ~~Ye, C., B. Yuan, Y. Lin, Z. Wang, W. Hu, T. Li, W. Chen, C. Wu, C. Wang, S. Huang, J. Qi, B. Wang, C. Wang, W.~~
629 ~~Song, X. Wang, E. Zheng, J. E. Krechmer, P. Ye, Z. Zhang, X. Wang, D. R. Worsnop, and M. Shao.: Chemical~~
630 ~~characterization of oxygenated organic compounds in the gas phase and particle phase using iodide CIMS with~~
631 ~~FIGAERO in urban air, *Atmos. Chem. Phys.*, 21, 8455-78, <https://doi.org/10.5194/acp-21-8455-2021>, 2021.~~

632 Yus-Díez, J., Bernardoni, V., Mocnik, G., Alastuey, A., Ciniglia, D., Ivancic, M., Querol, X., Perez, N., Reche, C.,
633 Rigler, M., Vecchi, R., Valentini, S., & Pandolfi, M.: Determination of the multiple-scattering correction factor and its
634 cross-sensitivity to scattering and wavelength dependence for different AE33 Aethalometer filter tapes: a multi-
635 instrumental approach, *Atmos. Meas. Tech.*, 14: 6335-55, <https://doi.org/10.5194/amt-14-6335-2021>, 2021.

636 Zeng, L. H., Zhang, A. X., Wang, Y. H., Wagner, N. L., Katich, J. M., Schwarz, J. P., Schill, G. P., Brock, C., Froyd,
637 K. D., Murphy, D. M., Williamson, C. J., Kupc, A., Scheuer, E., Dibb, J., and Weber, R. J.: Global Measurements of
638 Brown Carbon and Estimated Direct Radiative Effects, *Geophys. Res. Lett.*, 47, <https://doi.org/10.1029/2020gl088747>,
639 2020.

640 Zhang, Y., Albinet, A., Petit, J.-E., Jacob, V., Chevrier, F., Gille, G., Pontet, S., Chrétien, E., Dominik-Sègue, M.,
641 Levigoureux, G., Močnik, G., Gros, V., Jaffrezo, J.-L., and Favez, O.: Substantial brown carbon emissions from
642 wintertime residential wood burning over France, *Sci. Total Environ.*, 743, 140752,
643 <https://doi.org/10.1016/j.scitotenv.2020.140752>, 2020.

644 Zotter, P., H. Herich, M. Gysel, I. El-Haddad, Y. Zhang, G. Močnik, C. Hüglin, U. Baltensperger, S. Szidat, and A. S.
645 H. Prévôt. 2017.: Evaluation of the absorption Ångström exponents for traffic and wood burning in the Aethalometer-
646 based source apportionment using radiocarbon measurements of ambient aerosol, *Atmos. Chem. Phys.*, 17, 4229-49,
647 <https://doi.org/10.5194/acp-17-4229-2017>, 2017.

648

649

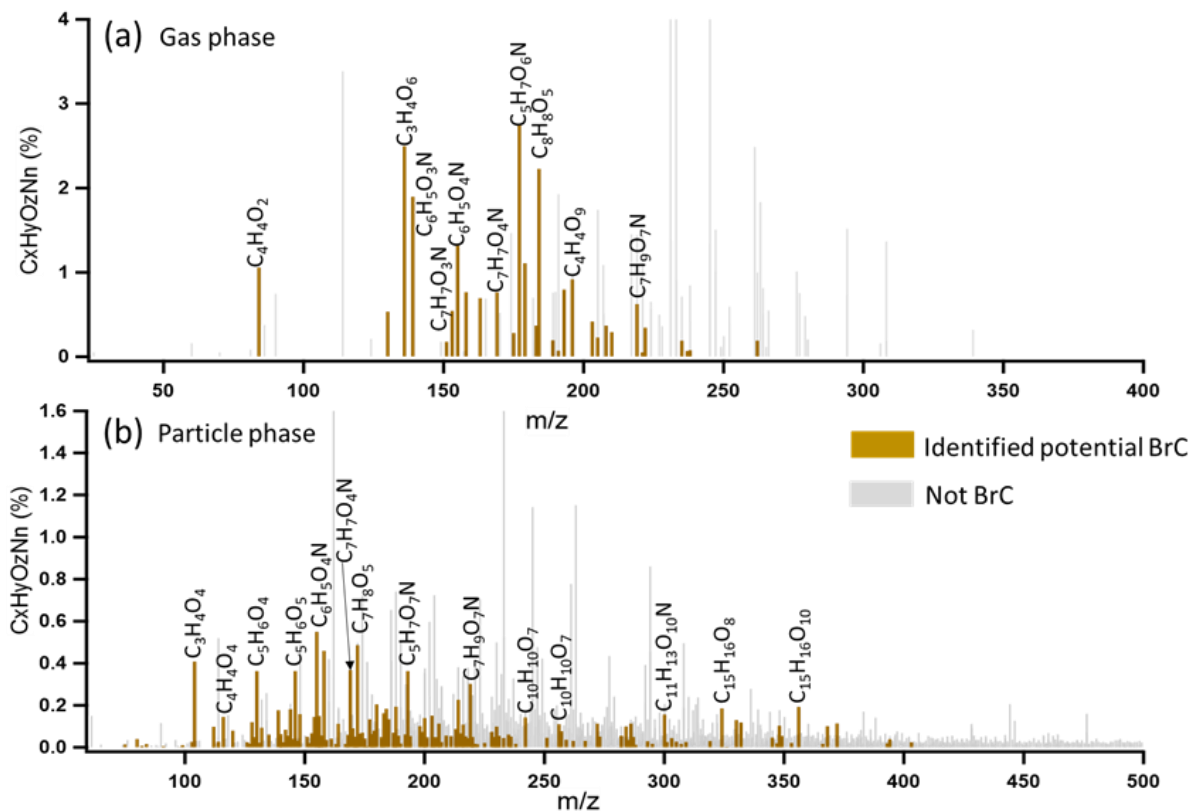
650

651

652

653

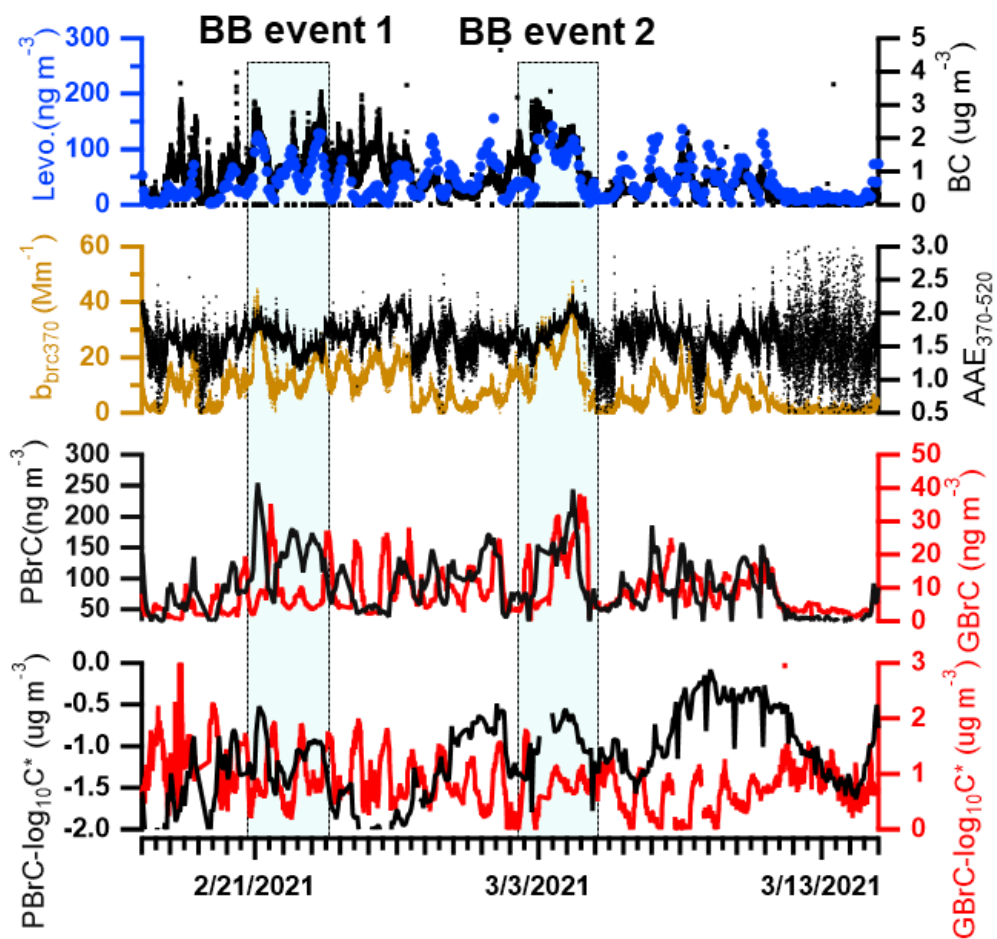
654



655

656 **Figure 1. CIMS mass spectra of organic aerosol measured by FIGAERO-CIMS for a biomass burning event on**
 657 **March 1st, 2021, a: gas phase, b: particle phase. The CI source employs reactions of I⁻ ions, which convert**
 658 **analyte molecules into [M+I]⁻ ions. Legends above MS features correspond to neutral molecules. The brown**
 659 **peaks in mass spectra were assigned as potential BrC molecules, while the gray peaks refer to the other organic**
 660 **molecules.**

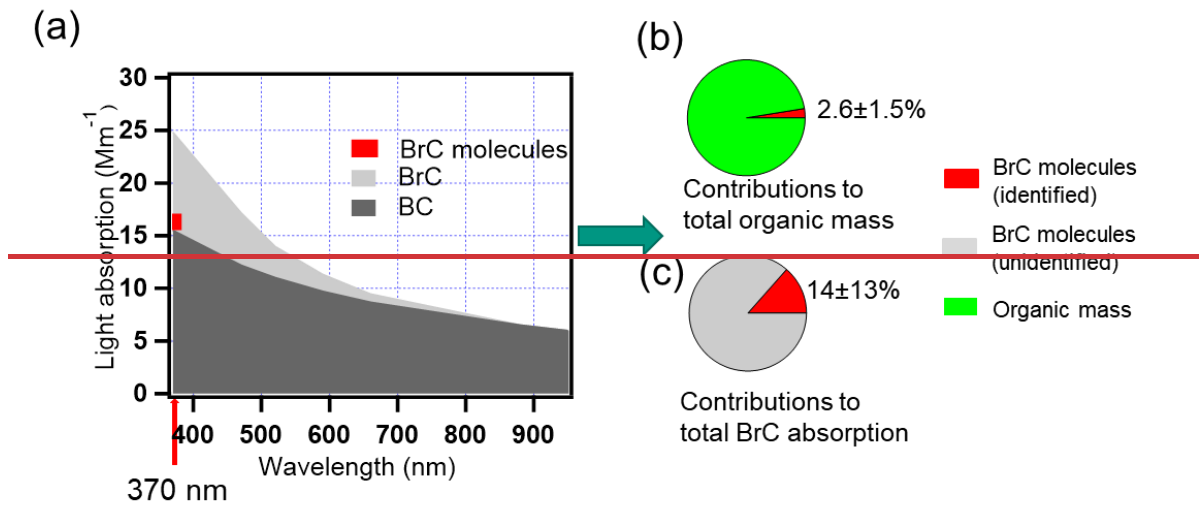
661



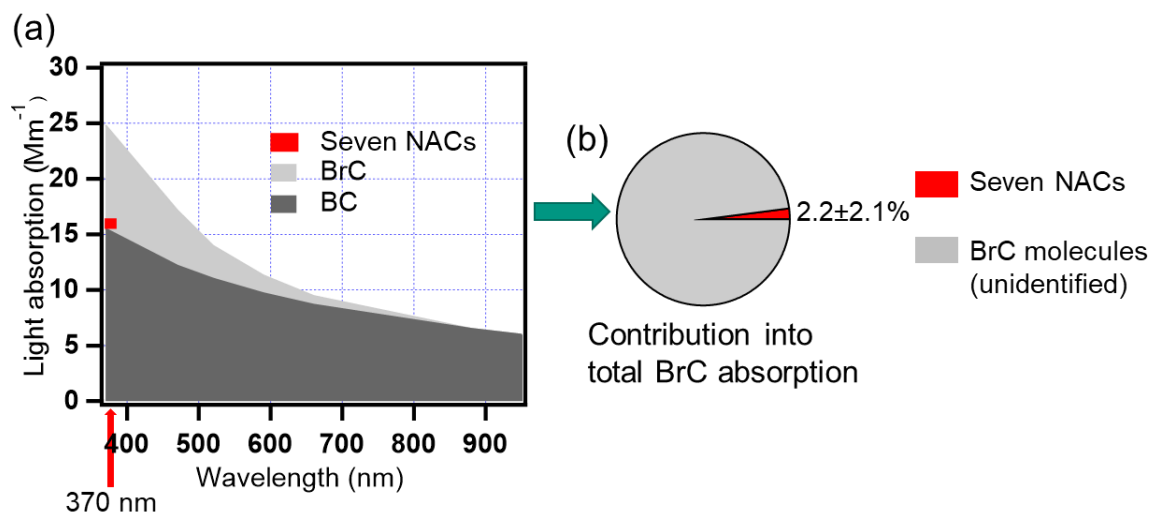
662
 663 **Figure 2.** Time series of levoglucosan (Levo.) concentrations in particle phase from FIGAERO-CIMS, BC
 664 concentrations from aethalometer (AE33), absorption of brown carbon at 370 nm (b_{bc370}), absorption Ångström
 665 exponents between 370 nm and 520 nm ($AAE_{370-520}$), brown carbon concentrations in particle phase (PBrC) and
 666 gas phase (GBrC) and volatility ($\log_{10}C^*$) of brown carbon in particle phase (PBrC_ $\log_{10}C^*$) and gas phase
 667 (GBrC_ $\log_{10}C^*$) during the winter campaign.

668

669



670

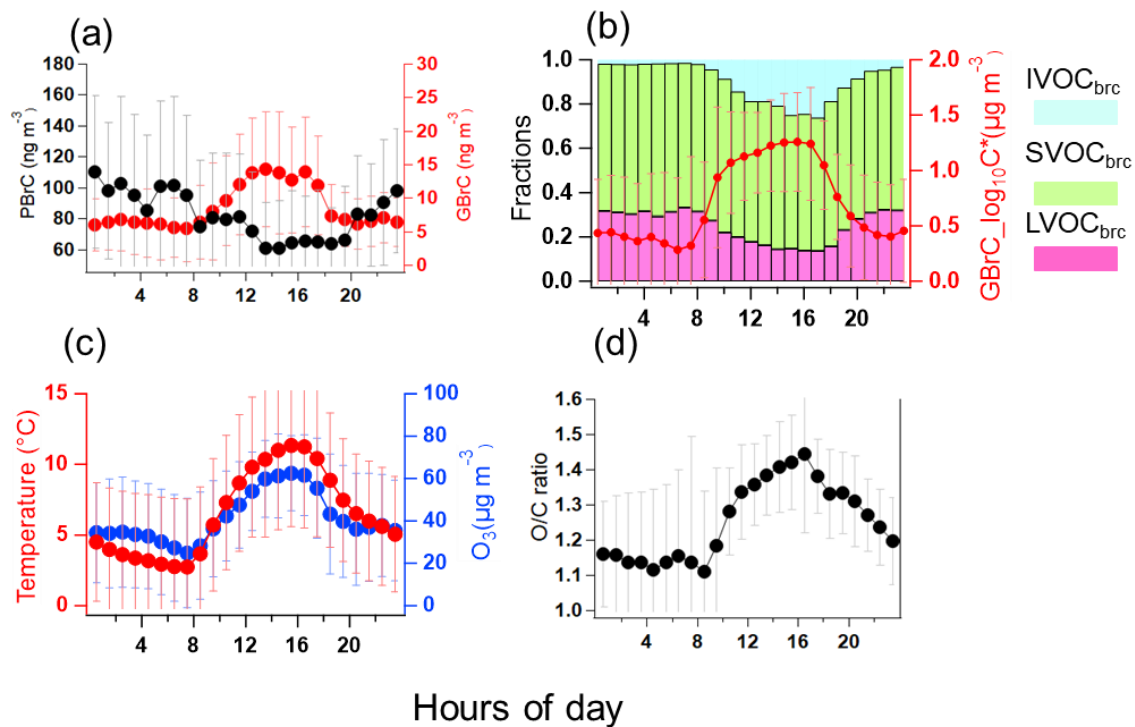


671

672 **Figure 3. (a) A stacked plot showing the main contributions to aerosol absorption from brown carbon and black**
 673 **carbon based on the seven wavelengths measured by the aethalometer AE33. The contribution of seven NACs**
 674 **the identified brown carbon molecules to the total aerosol absorption is indicated in red at 370 nm. (b) Average**
 675 **absorption contribution of seven NACs to total absorption by BrC. The red: seven NACs; the gray: unidentified-**
 676 **BrC molecules. (b) Average mass contribution of the potential BrC molecules to estimated total organic mass**
 677 **and (c) absorption contribution of the potential BrC molecules identified to total absorption by BrC. The red**
 678 **pie: identified BrC molecules; the gray pie: unidentified BrC molecules; the green pie: all organic mass.**

679

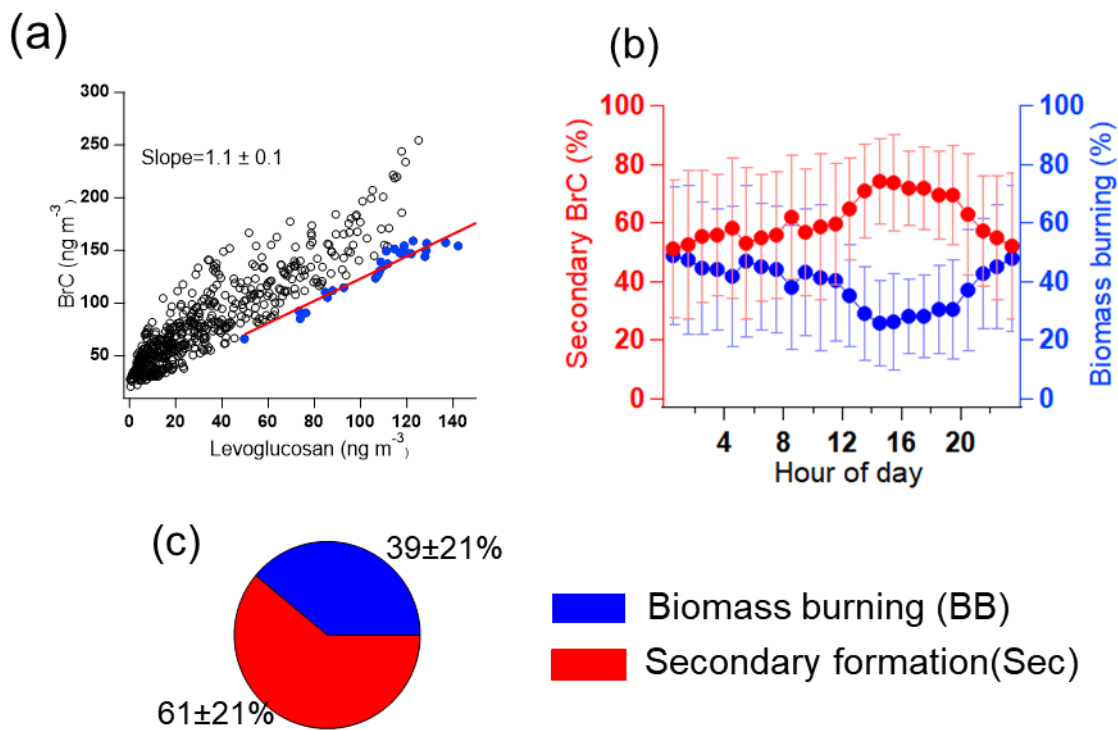
680



681
 682 **Figure 4. Diurnal profiles averaged over the whole winter campaign of (a) BrC in the particle (PBrC) and gas**
 683 **phase (GBrC), (b) BrC volatility fractions in LVOC_{brc}, SVOC_{brc}, IVOC_{brc}, and mean BrC volatility in the gas**
 684 **phase (red line), (c) temperature and ozone concentration. (d) O/C ratio of the oxidized organic components in**
 685 **the gas phase.**

686

687

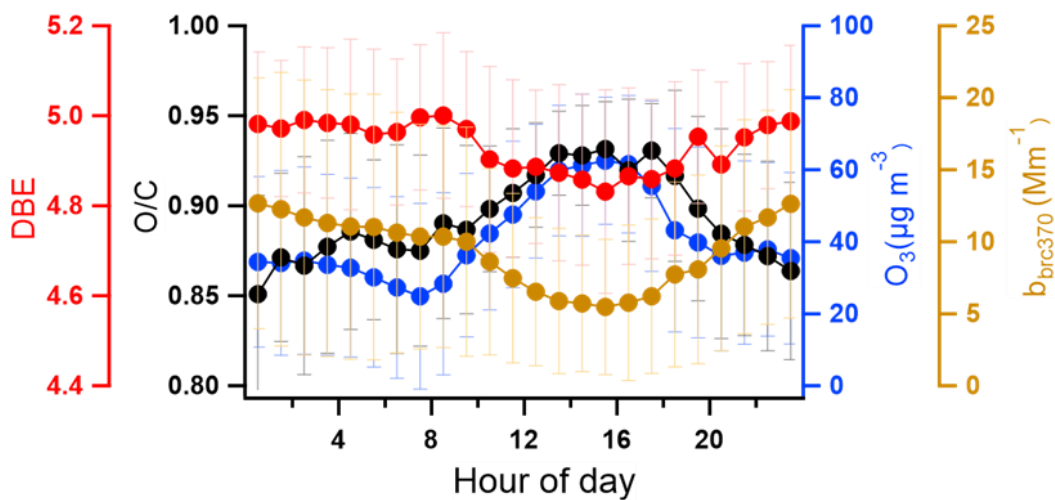


688
 689 **Figure 5. (a) Correlation analysis of BrC and levoglucosan in the particle phase for the analysis of the**
 690 **contribution of biomass burning using the edge method (Day et al., 2015). Blue points are the data used to**
 691 **determine [BrC/lev.]_{BB}. (b) diurnal profile of secondary-formation BrC and biomass-burning BrC for the whole**
 692 **measurement campaign. (c) Average mass fractions of secondary formed BrC and biomass-burning primary**
 693 **BrC for the whole campaign.**

694

695

696



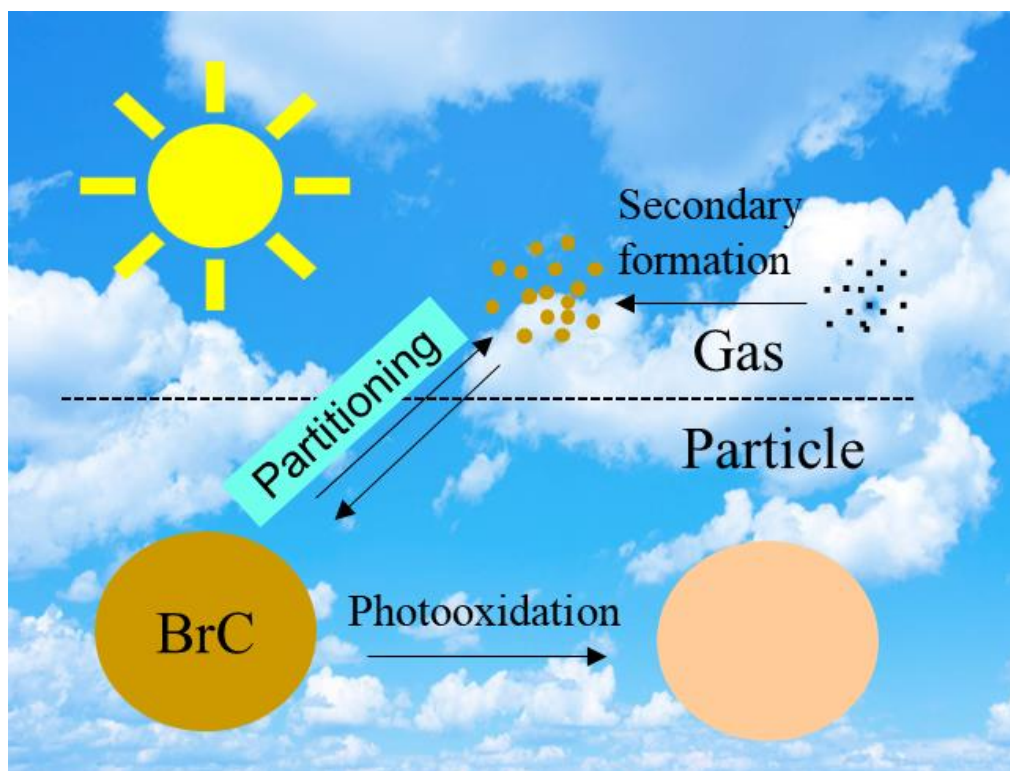
697

698 **Figure 6. The diurnal profile of DBE (double bond equivalent), O/C ratio of BrC, O₃, and b_{brc370} (absorption of**
699 **BrC at 370 nm) during the whole measured period.**

700

701

702



703

704 **Figure 7. A conceptual picture of the abstract**

705

706

707